NeuroImage: Clinical 19 (2018) 848–857

Contents lists available at ScienceDirect

NeuroImage: Clinical

journal homepage: www.elsevier.com/locate/ynicl

SPG11 mutations cause widespread white matter and basal ganglia abnormalities, but restricted cortical damage

Ingrid Faber[a], Alberto Rolim Muro Martinez[a], Thiago Junqueira Ribeiro de Rezende[a], Carlos Roberto Martins Jr.[a], Melina Pazian Martins[a], Charles Marques Lourenço[c], Wilson Marques Jr.[c], Celeste Montecchiani[d], Antonio Orlacchio[d,e], Jose Luiz Pedroso[f], Orlando Graziani Povoas Barsottini[f], Íscia Lopes-Cendes[b], Marcondes Cavalcante França Jr.[a,*]

[a] Department of Neurology, University of Campinas (UNICAMP), Campinas, Brazil
[b] Department of Medical Genetics, University of Campinas (UNICAMP), Campinas, Brazil
[c] Department of Neurology, University of São Paulo (USP-RP), Ribeirão Preto, Brazil
[d] Laboratorio di Neurogenetica, Centro Europeo di Ricerca sul Cervello (CERC) - Istituto di Ricovero e Cura a Carattere Scientifico (IRCCS) Santa Lucia, Rome, Italy
[e] Dipartimento di Scienze Chirurgiche e Biomediche, Università di Perugia, Perugia, Italy
[f] Department of Neurology, Federal University of São Paulo (UNIFESP), São Paulo, Brazil

ARTICLE INFO

Keywords:
Complicated hereditary spastic paraplegia
SPG11
Motor neuron disorder
Thinning of the corpus callosum
White matter
Grey matter
Spinal cord

ABSTRACT

SPG11 mutations are the major cause of autosomal recessive Hereditary Spastic Paraplegia. The disease has a wide phenotypic variability indicating many regions of the nervous system besides the corticospinal tract are affected. Despite this, anatomical and phenotypic characterization is restricted. In the present study, we investigate the anatomical abnormalities related to *SPG11* mutations and how they relate to clinical and cognitive measures. Moreover, we aim to depict how the disease course influences the regions affected, unraveling different susceptibility of specific neuronal populations. We performed clinical and paraclinical studies encompassing neuropsychological, neuroimaging, and neurophysiological tools in a cohort of twenty-five patients and age matched controls. We assessed cortical thickness (FreeSurfer software), deep grey matter volumes (T1-MultiAtlas tool), white matter microstructural damage (DTI-MultiAtlas) and spinal cord morphometry (Spineseg software) on a 3 T MRI scan. Mean age and disease duration were 29 and 13.2 years respectively. Sixty-four percent of the patients were wheelchair bound while 84% were demented. We were able to unfold a diffuse pattern of white matter integrity loss as well as basal ganglia and spinal cord atrophy. Such findings contrasted with a restricted pattern of cortical thinning (motor, limbic and parietal cortices). Electromyography revealed motor neuronopathy affecting 96% of the probands. Correlations with disease duration pointed towards a progressive degeneration of multiple grey matter structures and spinal cord, but not of the white matter. *SPG11*-related hereditary spastic paraplegia is characterized by selective neuronal vulnerability, in which a precocious and widespread white matter involvement is later followed by a restricted but clearly progressive grey matter degeneration.

1. Introduction

Hereditary spastic paraplegia (HSP) is a diverse group of rare single-gene disorders that share key clinical aspects: progressive lower limb spasticity and weakness (Harding, 1983; de Souza et al., 2017). Mutations affecting the *SPG11* gene are the major cause of Autosomal Recessive HSP accounting for approximately 25% of the cases (Kara et al., 2016). The disease has a wide phenotypic variability indicating many regions of the nervous system besides the corticospinal tract are affected, but the anatomical basis of the disease is not well elucidated (Pensato et al., 2014; Siri et al., 2010).

Neuroimaging techniques have proven to be a powerful tool in

Abbreviations: ACE-R, Addenbrooke's Cognitive Examination Revised; ALS, amyotrophic lateral sclerosis; CA, cord area; CE, cord eccentricity; CMAP, compound muscle action potential; CST, corticospinal tract; DTI, diffusion tensor imaging; FA, fractional anisotropy; GM, grey matter; HSP, hereditary spastic paraplegia; LH, left hemisphere; MD, mean diffusivity; MOCA, Montreal cognitive assessment; NPI, neuropsychiatric inventory; PNP, sensory-motor polyneuropathy; PNS, peripheral nervous system; RH, right hemisphere; ROI, region of interest; SC, spinal cord; SNAP, sensory nerve action potential; SPRS, Spastic Paraplegia Rating Scale; STS, cortex adjacent to the superior temporal sulcus; WM, white matter; WES, whole exome sequencing

* Corresponding author at: Department of Neurology, University of Campinas, R. Tessália Vieira de Camargo, 126, 13083-887 Campinas, Brazil.
E-mail addresses: mcfrancajr@uol.com.br, mfranca@fcm.unicamp.br (M.C. França).

https://doi.org/10.1016/j.nicl.2018.05.031
Received 17 February 2018; Received in revised form 20 May 2018; Accepted 22 May 2018
Available online 09 June 2018

many neurodegenerative disorders (Agosta et al., 2016; Hanganu et al., 2014). Such tools demonstrate *in vivo* structural abnormalities and provide a better understanding of the disease mechanisms and progression. Little is known about the extent of neurodegeneration in SPG11 patients and how it affects sequentially certain neuronal populations (França Jr et al., 2012; Pan et al., 2013).

Previous studies with limited number of patients have unraveled a diffuse pattern of White Matter (WM) microstructural integrity loss as well as basal ganglia atrophy. Most of these studies employed unimodal analyses focusing on WM tracts. Then, some unexplored aspects of the disease still deserve investigation, such as cortical and spinal cord involvement as well as potential correlations between clinical aspects and damage to specific brain regions (França Jr et al., 2012; Pan et al., 2013). In this scenario, we propose a comprehensive clinical, neuroimaging and neurophysiologic study regarding unexplored aspects of the disease in a cohort of 25 SPG11 patients. Our aim is first, to provide detailed genetic and clinical characterization concerning motor and cognitive aspects of the disease, correlating these findings with anatomical aspects. Moreover, we aim to delineate how the disease course influences the regions affected, unraveling different susceptibility of specific neuronal populations. To achieve these two objectives, we have applied robust neuroimaging tools to characterize unexplored anatomical aspects in the disease, such as cortical thickness, WM integrity, spinal cord area and morphometry.

2. Materials and methods

2.1. Subject's selection

Between 2013 and 2016, we enrolled 25 consecutive patients with confirmed *SPG11* mutations regularly followed at UNICAMP neurogenetics outpatient clinic. They came from 16 unrelated families. Molecular diagnosis was performed by Sanger and/or Whole Exome Sequencing (WES). Subjects underwent neurological, neurophysiological and neuroimaging examination as detailed below. None had associated neurological or systemic diseases.

Twenty-five age and sex matched healthy individuals were also included as a control group for neuroimaging analyses. None of them had past personal or family history of neurological disease.

This study was approved by our institution review board (CAAE 48122515.7.0000.5404), and all probands or their parents signed an informed consent before any study-related procedure.

2.2. Clinical and genetic assessment

Patients underwent a comprehensive neurological evaluation at the University of Campinas outpatient clinic: they were assessed for type and age of the first symptoms, associated neurological and clinical features. Cognitive disability, learning difficulties, as well as the presence of progressive cognitive deterioration were evaluated trough the Addenbrooke's Cognitive Examination Revised (ACE-R). The ACE-R is a comprehensive neuropsychological tool that has been validated for the Brazilian population. The score ranges from 0 to a maximum of 100 points (lower scores indicate greater impairment) and encompasses 5 cognitive domains: attention/orientation, memory, fluency, language and visuospatial abilities (Mioshi et al., 2006; Carvalho and Caramelli, 2007). Neuropsychiatric disturbances were explored through the neuropsychiatric inventory (NPI), a brief interview with the patient's main caregiver designed to detect behavioral issues such as anxiety, depression, and delusional thoughts (Cummings et al., 1994). Disease severity was quantified through detailed neurological assessment as well as the Spastic Paraplegia Rating Scale (SPRS) that ranges from 0 (no abnormalities) to 52 (Schüle et al., 2006). Such assessment was performed two times in 21/25 patients across a mean interval of 12 months (standard deviation: ± 2.06). The difference between the two SPRS measurements was used to assess the disease's rate of progression. All scales and examinations were performed by a single investigator (IF). For the genetic diagnosis, standard Sanger sequencing of the coding sequences and flanking intronic regions was performed in 13 families. WES was performed in five families (in two families one individual was submitted to Sanger and the other to WES). Methodological data on genetic diagnosis is available as supplemental material.

2.3. MRI acquisition and protocol

A 3 T Achieva PHILIPS scanner with a standard 8 channel head coil was used to scan all patients and controls. The exams were performed at the same day of the clinical evaluation. To exclude incidental findings, routine T1 and T2 weighted sequences were performed for all subjects. We obtained T1 weighted volumetric images covering the whole brain and the cervical spinal cord with the following acquisition parameters: sagittal orientation, voxel matrix $240 \times 240 \times 180$, voxel size $1 \times 1 \times 1\,mm^3$, TR/TE 7/3.201 ms, flip angle 8°. These T1-weighted images were used to measure spinal cord area/eccentricity, cortex thickness and deep GM volumes.

We also acquired a Gradient Echo Diffusion tensor imaging (DTI) sequence as follows: axial orientation, $2 \times 2 \times 2\,mm^3$ acquiring voxel size, interpolated to $1 \times 1 \times 2\,mm^3$; reconstructed matrix 256×256; 70 slices; TE/TR 61/8500 ms; flip angle 90; 32 gradient directions; no averages; max b-factor = $1000\,s/mm^2$; six-minute scan. The DTI images were used for analysis of WM integrity.

2.4. Image processing

2.4.1. Cerebral grey matter

2.4.1.1. Cortical thickness (n = 20 patients and controls). Cortical thickness was computed using the FreeSurfer software v.5.3. This tool is more sensitive to assess cortical damage than measures of area or volume (Hutton et al., 2009). Measurements were performed according to the protocol suggested by Fischl and Dale (2000) and have been previously detailed by our group (De Rezende et al., 2015). The software creates triangle meshes that form two surfaces, the interface between Grey Matter (GM) and cerebrospinal fluid (CSF) and the interface between GM and White Matter (WM). The shortest distance between the interfaces constitutes the measured cortical thickness. For comparisons, we followed the cortical regions as defined by Desikan et al. (2006). Five patients had their images excluded due to major segmentation errors. Those concerned patients with grossly enlarged ventricles due to ex vacuo atrophy and the main errors regarded labelling of lateral ventricles as WM or GM. Further FreeSurfer analyses were therefore performed with 20 patients and 20 controls.

2.4.1.2. Basal ganglia volumes (n = 21 patients and controls). T1 weighted images were processed with the T1 MultiAtlas approach using "MRICloud" (MRICloud.org), a public web-based service for multi-contrast imaging segmentation and volumetric quantification. T1 MultiAtlas provides an accurate and reliable segmentation of deep structures. Raw images were re-oriented (sagittal to axial), corrected for inhomogeneity and the whole brain was segmented after skull-stripping. Linear and non-linear algorithms (Miller et al., 2013) for brain co-registrations and a multi-atlas labeling fusion was employed to identify brain regions followed by a last step of labelling adjusting with PICSL (Tang et al., 2014). Nineteen atlases (JHU adult atlas version 9B) were used to generate 283 structural definitions (Wu et al., 2016). From these labels we were primarily interested in determining deep GM volumes. All analyses were performed in native space. The computations were processed on the Gordon cluster of XSEDE (Towns et al., 2014). Images from 4 patients were excluded due to minor segmentation errors. These occurred in the same patients in which FreeSurfer performed an inaccurate labelling with the exception of one patient whose image was successfully processed by T1-MultiAtlas but not by FreeSurfer. The paired controls were excluded with the objective

of maintaining homogeneous groups.

2.4.2. Cerebral white matter

2.4.2.1. DTI multi-atlas (n = 24 patients and controls). WM microstructural damage was assessed through the DTI-MultiAtlas, processed using "MRICloud", where Raw DTI-weighted images were co-registered and corrected for eddy currents and subject motion using a 12-parameter affine transformation (Zhuang et al., 2006). The DTI-parameters (Fractional Anisotropy (FA), Axial diffusivity, Mean Diffusivity and Radial Diffusivity) were calculated using a multivariate linear fitting and skull-stripped using the b = 0 image, by intensity threshold, a tool of ROI Editor software. This preprocessing was performed using DTIStudio software (Jiang et al., 2006). After that, a non-linear registration using a multi-contrast LDDMM was performed, followed by the parcellation, which employs a DLFA algorithm (Tang et al., 2014). Eight atlases (*JHU adult atlas version 1*) were used to generate 168 structures. One patient and the paired control were excluded from this analysis due to segmentation artifacts. All analyses were performed in native space. The computations were processed on the Gordon cluster of XSEDE (Towns et al., 2014).

2.4.2.2. Corpus callosum and fornix volumes (n = 21 patients and controls). T1 weighted images were processed with the T1 MultiAtlas approach as previously described for deep grey matter structures. We then obtained the volumes for the corpus callosum (divided into 5 portions: rostrum, corpus, splenium, right and left tapetums) and the fornix (divided into two portions at each side: fornix and stria terminalis).

2.4.3. Spinal cord morphometry (n = 25 patients and controls)

Spineseg is a robust software that requires minimal interaction and corrects common caveats in the study of the Cervical SC, such as the imaging angle and neck position variations that otherwise hamper a precise definition of area and morphology. The only interactive step consists of imputing a few nodes that define an approximation of the spine and neck curvature, after which SC boundaries are segmented automatically by tree pruning, fitting an ellipse to the segmented boundaries. Three consecutive ellipses were sampled between C2 and C3 intervertebral discs and a mean value was obtained for SC area (CA), expressed in mm^2, and eccentricity (CE). CE is defined as the square root of $1 - (a / b)^2$, where a is the smaller and b is the larger diameter of the SC. In summary, CE is a measure of antero-posterior flattening. Disorders affecting the posterior columns, such as Friedreich's Ataxia, are associated with cord flattening, whereas amyotrophic lateral sclerosis (ALS), affecting selectively lateral columns, does not lead to morphology changes (Branco et al., 2014).

2.5. Neurophysiological assessment (n = 25)

Nerve conduction studies (NCS) and monopolar electromyography (EMG) testing were performed by standard procedures on a Nihon Kohden device (Neuropack MEB-9200 Electromyographer, Japan) (França Jr et al., 2008). NCS employed supramaximal stimulation and surface electrodes recording. Surface body temperature was controlled (32–34 °C). Compound muscle action potential (CMAP) evaluation included bilateral median, ulnar, fibular and tibial nerves and was performed through orthodromic conduction. Sensory nerve action potentials (SNAP) were obtained antidromically at the median, ulnar, radial and sural nerves bilaterally. F-waves were captured at the ulnar and tibial nerves. EMG encompassed at least one proximal and one distal appendicular muscle at all four limbs as well as cranial and paravertebral muscles (thoracic and lumbar). Insertional and rest activity were analyzed semi quantitatively for 5 min at four different points at each muscle. Morphology of motor unit action potentials was recorded during slight, intermediate, and maximum voluntary contraction.

The sural/radial nerve amplitude ratio (SRAR) was calculated to increase the diagnostic yield of sensory-motor polyneuropathy (PNP). The rationale behind this quotient is that sural SNAP will decrease in a more pronounced manner than the radial SNAP in a length-dependent process, therefore decreasing SRAR. Rutkove and colleagues originally proposed a 0.4 cutoff value, but future investigators have found a 0.2 cutoff to be more precise (Rutkove et al., 1997; Oberbeek et al., 2005). Therefore, values > 0.2 argue against PNP. We were also interested in investigating the split hand index, a quotient devised to increase diagnostic specificity in ALS. It is calculated by multiplying the amplitudes of abductor pollicis brevis and first dorsal interosseus and dividing this product by the abductor digiti minimi amplitude. The rationale for this calculation lies in the preferential involvement of the thenar eminence and the relative sparing of hypothenar eminence in ALS. An index of 5.2 or less is in agreement with ALS phenotype (74% sensitivity and 80% specificity) (Menon et al., 2013). To quantify peripheral SPG11-related burden, we have scored clinically meaningful atrophy as ranging from 0 (absent), 1 (present in upper or lower distal limbs) to 2 (present in 4 limbs).

2.6. Statistical analysis

Statistical analyses were performed using the IBM SPSS statistics version 20. Clinical and demographic data of all subjects are reported with descriptive statistics. MRI analyses included both group comparisons and assessment of correlations and all were corrected for multiple comparisons as detailed below. Level of significance was set at $p < 0.05$ for all analyses.

2.6.1. Group comparisons (patients versus controls)

All imaging techniques were assessed through a General Linear Model. Age and gender were used as covariates. For cortical thickness and brain volumetric studies, estimated intracranial volume was also added as a covariate. In order to correct for multiple comparisons, we employed the Dunn-Sidak adjustment.

2.6.2. Correlations

Pearson correlation coefficient assessed possible correlations between imaging measures and clinical data whenever data distribution was normal, Spearman correlations were employed for data not normally distributed. Gender was used as a covariate for correlations, but age was not, given the interest in studying its relationship to the outcomes. Dunn-Sidak correction was employed to adjust for multiple comparisons.

3. Results

3.1. Clinical, neuroimaging and neurophysiological characterization of the phenotype

3.1.1. Clinical features and genetic profile

Mean age and disease duration were 29 (range 18–49) and 13.2 (range 0–30) years, respectively. Twelve were men. There was no difference regarding age ($p = 0.89$) and gender ($p = 1$) between patients and controls. Progressive spastic paraplegia was the main symptom in all cases, with gait disturbances beginning on average at 16.36 (range 5–25) years (Table 1). All patients had pyramidal signs, urinary incontinence or urgency and reduced blinking velocity with subtle hypomimia. Sixteen (64%) were wheelchair bound, which happened after a mean disease duration of 13.8 years. The disease's annual rate of progression across 1 year was of 3.65 points in the SPRS scale. In regard to spasticity subscores (range 0–8) the rate of worsening was of 1.14 point annually. Severe amyotrophy of intrinsic hand muscles was present in ten (40%). Eighteen (72%) probands had history of learning difficulties before the onset of gait disturbances, while five (20%) reported delay or mild abnormalities during gait acquisition such as an equine posture or tip toe gait. Frequency of phenotypical traits is

Table 1
Demographic, clinical, cognitive and genetic data of SPG11 patients.

Patient no.	Gender	Age of onset	Disease duration	Age	SPRS	ACE-R	VLOM	Learning difficulties	Obesity	Parkinsonism	Ataxia	Pathological laughter	Mutation	Other features
F1.1	M	11	13	24	37	58	1.62	+	+	+		+	c.118C > T	Epilepsy, fecal incontinence, rest tremor
F1.2	M	19	3	22	23	56	1.21	+			+	+ +	c.118C > T	
F2	F	11	15	26	43	32	1.13	+		+	+	+ +	c.529_533delATATT	
F3	M	14	21	35	32	32	1.38	+				+ +	c.733_734delAT	ALS-like, facial dystonia
F4	F	15	12	27	32	35	1			+	+	+ +	c.A7256G/c.733_734delAT	Hand amiotrophy
F5	F	13	13	26	21	80	1.47	+	+			+ +	c.118C > T	Hand amiotrophy
F6.1	F	21	3	24	18	86	1.56		+				c.118C > T/c.1162C > A	
F6.2	F	18	0	18	5	88	1.40	+	+				c. 118C > T/c.C1162A	
F7	M	21	6	27	15	76	1.13	+				+	c. 118C > T	Pes cavus, hand amiotrophy
F8.1	F	15	14	29	37	57	1.06	+	+		+	+ +	c. 529_533delATATT/c. 2656T > C	Postural tremor
F8.2	M	16	7	23	19	47	1.27	+			+	+	c. 529_533delATATT/c. 2656T > C	
F9	M	9	21	30	37	65	1.5			+	+	+ +	c.118C > T/c.1951C > T	Hallucinations, agressiveness
F10.1	F	18	24	42	40	32	2.5				+	+ +	c.1951C > T/c.3809T > A	Hypophonia, hallucinations
F10.2	F	20	24	44	48	27	1.25				+	+ +	c.1951C > T/c.3809T > A	Hypophonia, dysphagia, postural tremor
F10.3	M	15	15	30	25	82	1.89				+	+	c.1951C > T/c.3809T > A	
F10.4	F	20	30	50	40	10	0.2	+			+	+ +	c.1951C > T/c.3809T > A	Hypophonia, dysphagia with gastrectomy, strabismus
F11.1	M	25	11	36	34	58	1.64		+			+ +	c118C > T/c.4264C > T	Hand amiotrophy, agressiveness
F11.2	F	25	7	32	38	46	1.15	+	+			+ +	c118C > T/c.4264C > T	
F12.1	M	16	13	29	37	36	2.83	+		+		+	c.1951C > T/c.3809T > A	Hallucinations, postural tremor
F12.2	F	19	11	30	36	42	2.25				+	+	c.1951C > T/c.3809T > A	Strabismus
F13.1	M	15	8	23	27	50	1.33	+		+			c.118C > T	Rubral tremor
F13.2	M	18	3	21	10	56	1.58	+					c.118C > T	Epilepsy
F14	F	13	19	32	45	33	1.22		+	+		+ +	c.704_705delAT	Cervical dystonia, upper limb spasticity
F15	M	10	14	24	36	64	1.38		+		+	+ +	c.733_734delAT/c. 5490delT	Facial dystonia
F16	F	5	23	28	37	34	0.90	+	+			+	c.2444 + 1G > C/ c.442 + 1G > C	Postural tremor, hand amiotrophy, fecal incontinence

Abbreviations: No. = number; F = family; M = male; F = female; SPRS = Spastic Paraplegia Rating Scale; ACE-R = Addenbrooke's Cognitive Examination Revised; VLOM comprises the ratios of the scores = verbal fluency plus language to orientation plus delayed recall memory (V.L.)/(O.M.).

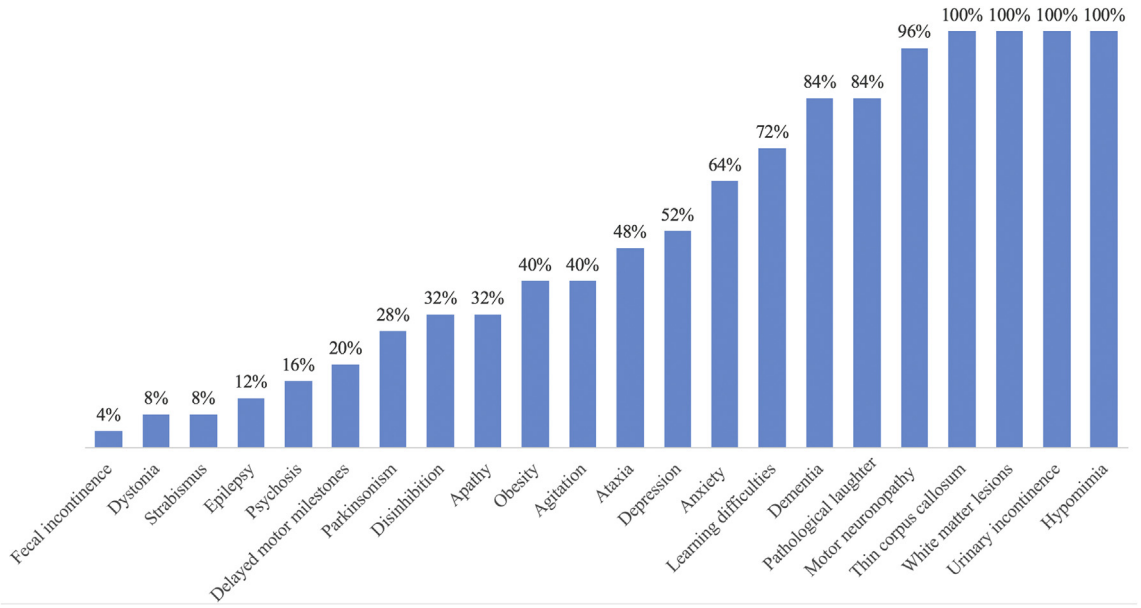

Fig. 1. Frequencies of phenotypic traits identified in 25 SPG11 patients.

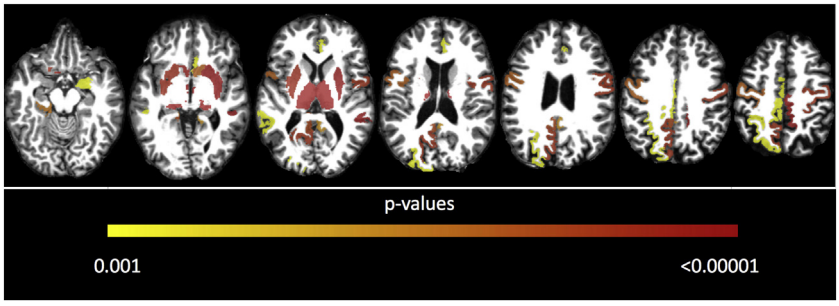

Fig. 2. Axial MR showing regions with significant GM damage in SPG11, areas are color-coded (from red to yellow). ROI-based analyses using T1 multi-atlas approach to assess deep GM volumes; FreeSurfer analyses of cortical regions as defined by Desikan et al. (2006) to assess cortical thickness. (For interpretation of the references to color in this figure legend, the reader is referred to the web version of this article.)

further detailed in Fig. 1.

Twenty-one (84%) patients fulfilled criteria for dementia (ACE-R score < 78 if > 11 years of schooling or < 68 in patients with < 11 years of schooling) (Carvalho and Caramelli, 2007). Mean ACE-R was 51.28 (range 10–88). Eighty-four was the mean score in the non-demented group, whereas the affected patients scored 45 points on average. From ACE-R subscores, verbal fluency was the most affected domain (mean score of 28%) followed by memory (45%), language (55%), attention and orientation (61%), and visuospatial abilities (65%). The sum of verbal fluency and attention was interpreted as an estimate of executive function. ACE-R has a subscore, the VLOM ratio, which has been shown to be useful in differentiating frontotemporal dementia and Alzheimer's disease. A VLOM ratio of < 2.2 points to frontotemporal dysfunction with 95% of specificity. A score of > 3.2, on the other hand, points to a dementia that resembles Alzheimer's disease (Mioshi et al., 2006). Twenty-three patients (92%) had a score of < 2.2 while the remaining three had indexes in the unspecific range. This indicates that frontotemporal dysfunction constitutes the clinical phenotype of dementia in SPG11. ACE-R correlated inversely with physical burden measured by the SPRS ($r = -0.70$, $p < 0.001$), reasoning that demented patients have an overall worse status.

In eleven families Sanger sequencing was the primary diagnostic method, whereas WES was performed in six (França Jr et al., 2012; Faber et al., 2017). Of the 16 families in our cohort, seven had at least one allele with a previously described nonsense mutation affecting *SPG11* gene (c.118C > T), with four homozygous and three compound heterozygous kindreds. Interestingly, all these patients or their ancestors came from the same small village in the northeast of Brazil (city of Brumado state of Bahia) (Stevanin et al., 2007). We were able to identify two new variants affecting two distinct families. A missense (c.1162C > A) and nonsense mutation (c.4264C > T) affecting respectively families 6 and 11 and both segregating with the phenotype. They were not present in multiple databases (Exac, 100 genomes) and were predicted to be pathogenic according to *in silico* softwares (Mutation Taster, Poliphen-2, SIFT) (Hamosh et al., 2013; Richards et al., 2015) (Table 1).

3.1.2. Cerebral grey matter

Significant differences in cortical thickness between patients and controls involved bilateral motor cortices including precentral and paracentral gyri; limbic structures: cingulate gyri (rostrum-anterior, posterior and isthmus) and left parahippocampal gyrus; as well as few associative areas: bilateral superior temporal sulcus (STS), left precuneus and superiorparietal cortices (Fig. 2).

In correlation analyses we were interested in the relationship of the motor cortices with the SPRS as well as of the associative cortices with cognition. The SPRS scores showed a significant inverse correlation with cortical thickness of precentral (right $r = -0.57$, $p = 0.008$; left $r = -0.62$, $p = 0.007$) and paracentral (right $r = -0.59$, $p = 0.006$; left $r = -0.67$, $p = 0.002$) cortices bilaterally. The ACE-R displayed significant positive correlation with the following areas: STS bilaterally (right $r = 0.65$, $p = 0.005$; left $r = 0.72$, $p = 0.002$) as well as left superior parietal ($r = 0.66$, $p = 0.009$) and precuneus ($r = 0.72$, $p = 0.002$) cortices.

Significant volumetric reduction of deep grey matter volumes was identified through T1-MultiAtlas. Volumes of bilateral thalamus (right and left $p < 0.001$), accumbens nucleus (right $p = 0.003$; left $p < 0.001$), putamen (right $p < 0.001$; left $p = 0.001$) and substantia

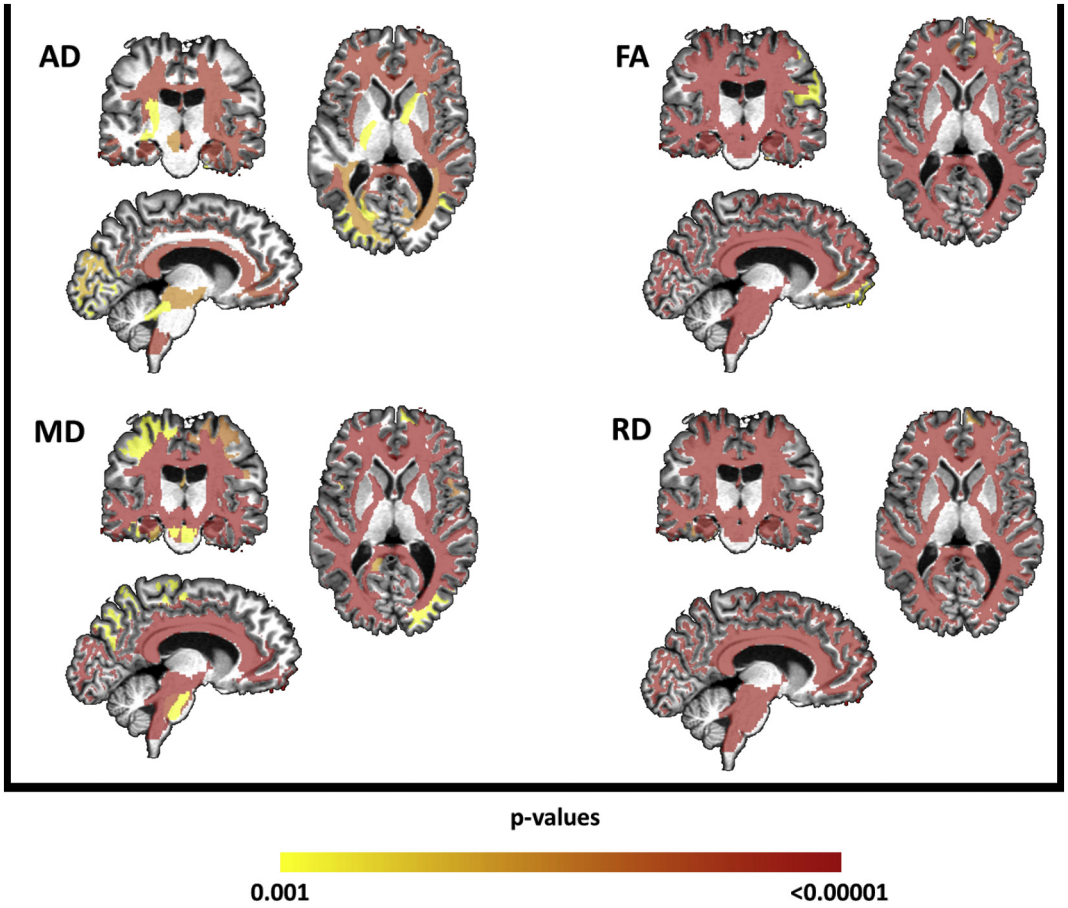

Fig. 3. Results of multi-atlas approach showing areas of reduced fractional anisotropy (FA) and increased axial diffusivity (AD), mean diffusivity (MD) and radial diffusivity (RD) in patients with SPG11 after comparison with controls, areas are color-coded (from red to yellow). (For interpretation of the references to color in this figure legend, the reader is referred to the web version of this article.)

nigra (right and left $p < 0.001$) as well as right amygdala ($p = 0.014$) and left red nucleus ($p = 0.012$) were significantly reduced in comparison to the control group (Fig. 2).

Volumes of both thalami (right $r = -0.612$, $p = 0.031$; left $r = -0.624$, $p = 0.024$) and accumbens nuclei (right $r = -0.63$, $p = 0.021$; left $r = -0.64$, $p = 0.017$) as well as left red nucleus ($r = -0.734$, $p = 0.001$), right putamen ($r = -0.65$, $p = 0.016$) and substantia nigra ($r = -0.59$, $p = 0.042$) correlated negatively with SPRS scale. ACE-R scale correlated with right thalamus volume ($r = 0.611$, $p = 0.032$) (Fig. 2).

3.1.3. Cerebral white matter

All WM tracts revealed significantly altered FA, MD, AD and RD values in patients compared to controls, indicating widespread WM microstructural damage (Fig. 3).

Using DTI atlas-based analysis, we first assessed whether CST diffusivity results correlate with motor handicap. Nonetheless no subpart of the CST correlated significantly with SPRS. Afterwards, we looked at the correlation between corpus callosum/fornices DTI and cognitive functioning. We indeed found that ACE-R scores correlated directly with FA in the following regions: bilateral fornices (right $r = 0.8$, $p < 0.001$; left $r = 0.58$, $p = 0.032$), right stria terminalis ($r = 0.75$, $p < 0.000$) and bilateral tapetums (right $r = 0.68$, $p = 0.002$; left $r = 0.58$, $p = 0.032$). Executive function also correlated with bilateral fornices (right $r = 0.71$, $p < 0.001$; left $r = 0.67$, $p = 0.004$), stria terminalis (right $r = 0.81$, $p < 0.001$; left $r = 0.62$, $p = 0.015$) and tapetums (right $r = 0.8$, $p < 0.001$; left $r = 0.67$, $p < 0.05$) while memory correlated with right fornix ($r = 0.8$, $p < 0.001$) and right stria terminalis ($r = 0.65$, $p < 0.006$).

Corpus callosum volume measured by T1 Atlas Based Analysis was reduced throughout all its subdivisions (Rostrum, Corpus, Splenium and Tapetums) as well as the stria terminalis bilaterally. Despite that, only stria terminalis volume correlated with ACE-R subscore for executive function ($r = 0.63$, $p = 0.024$).

3.1.4. Spinal cord

SC area was significantly reduced in SPG11 (Mean CA controls = 69.4 ± 7.4 mm^2 and patients = 51.9 + −6.1 mm^2, $p < 0.001$) without changes in eccentricity (Mean CE controls = 0.776 ± 0.009 Mean CE patients = 0.783 ± 0.009, $p = 0.362$). SPRS correlated inversely with CA ($r = -0.482$, $p = 0.015$).

3.1.5. Neurophysiological results

We were able to observe an axonal, motor and non-length dependent dysfunction affecting 24/25 patients. Conduction Velocities (CV) and distal latencies were essentially normal in motor and sensory studies. Amplitudes were mostly spared in sensory nerve action potentials (SNAPs). Compound muscle action potentials (CMAPs), on the other hand, revealed reduced amplitudes in 76%, with 36% of the probands revealing significant amplitude asymmetries. During myographic studies all affected individuals displayed chronic neurogenic changes (CNC) involving lower as well as upper extremities. CNC affected also the cranial segment in 55%. Abnormal spontaneous activity was found in 24% (Table 2).

Our data reveal a disproportion between sensory and motor abnormalities. From 100 SNAPs, only 7 were abnormal (3 were absent radial responses related to technical difficulties due to upper limb

Table 2
Major electrodiagnostic findings of SPG11 patients.

Patient	CMAP ra	SNAP ra	Assymetries	Appendicular CNC	Cranial CNC	Acute denervation
F1.1	+	+	+	+		
F2	+			+	+	+
F3	+	+	+	+		+
F4	+		+	+		+
F1.2	+			+	NP	
F5	+		+	+		+
F6.1				+		
F6.2				+		
F7	+		+	+		
F8.1	+		+	+	+	
F8.2	+		+	+	+	
F9	+			+	+	+
F10.1	+			+		
F10.2	+		+	+	+	+
F10.3				+	NP	
F10.4	+			+	+	
F11.1	+			+	+	
F11.2	+			+	+	
F12.1	+			+	+	
F12.2	+	+		+	+	
F13.1						
F13.2				+		
F14	+		+	+	+	
F15			+	+	+	
F16	+			+		

Abbreviations: CMAP = compound muscle action potential; ra = reduced amplitudes; SNAP = sensory nervous action potential; CNC = chronic neurogenic changes; NP = not performed.

spasticity). The only patient that had absent sural responses had significant foot deformities, so that the lack of response might be due to technical reasons. This hypothesis is reinforced by the lack of reduction of SNAP amplitudes in the upper limbs that were well higher than the lower normal limits (right median and ulnar amplitudes: 51.2 and 46.5 μV respectively). We were able to calculate the SRAR in 22 patients (one patient had absent sural responses as previously described and 2 had severe upper limb spasticity that hampered our ability to detect radial SNAPS), and we obtained ratios higher than 0.2 in all probands, arguing against a length dependent PNP.

Considering the striking abnormalities observed in the motor studies, it is useful to stress that CMAP amplitudes were lower in the upper limbs in comparison with lower limbs in 76%. When added to the high frequency of asymmetries observed, those abnormalities reveal a multifocal pathological process. The split-hand index was consistent with the ALS-pattern of thenar predominant atrophy (ratio < 5.2) in 15 (60%) patients.

As stated, needle myography disclosed large and long duration potentials in 24/25 patients (96%) all of whom displayed chronic neurogenic changes affecting at least upper and lower extremities. In 12/22 (54.5%) individuals tested, bulbar myotomes displayed chronic neurogenic changes as well. Four patients displayed signs of acute denervation. There was no clear distal-proximal gradient and in 3 there were significant asymmetries. Jointly, nerve conduction and EMG changes indicated a predominantly chronic, multifocal and exclusively motor neuropathy. Such a neurophysiologic pattern is consistent with a pathological process affecting the lower motor neuron cell bodies at the anterior horn.

3.2. Insights into disease course

3.2.1. Clinical results

SPRS scores had a significant association with disease duration ($r = 0.71$, $p < 0.001$). Cognitive performance, measured through the ACE-R score, also correlated inversely with disease duration ($r = -0.59$, $p = 0.002$).

3.2.2. Cerebral GM

Thickness at both precentral (right $r = -0.52$, $p = 0.037$; left $r = -067$, $p = 0.012$) and left paracentral cortices ($r = -0.67$, $p = 0.002$) correlated negatively with disease duration. In terms of basal ganglia volumetry, inverse correlation with disease duration was identified at putamens (right $r = -0.73$, $p = 0.002$; left $r = -0.63$, $p = 0.02$) and accumbens nucleus (right $r = -0.63$, $p = 0.023$; left $r = -0.61$, $p = 0.03$).

3.2.3. Cerebral WM

In contrast to GM, none of the WM metrics (DTI and/or volumes) displayed correlation with disease duration.

3.2.4. Spinal cord morphometry

Correlation analyses revealed reduced CA in patients with longer disease duration ($r = -0.531$, $p = 0.006$), supporting a progressive atrophy of the SC.

3.2.5. Neurophysiological results

Correlation analysis indicated more significant atrophy in patients with longer disease duration ($r = 0.71$, $p < 0.001$) and older age ($r = 0.85$, $p < 0.001$).

4. Discussion

The core clinical phenotypic features of SPG11 have been previously described (Kara et al., 2016; Hehr et al., 2007; De Bot et al., 2013). The novel contributions of the present study are not only to provide the detailed characterization of the structural signature of SPG11, but also to investigate how specific patterns of brain and spinal cord damage correlate with clinical manifestations. To accomplish these goals, we were able to collect a large sample of patients that underwent systematic motor and cognitive assessment combined with multimodal MRI evaluation and neurophysiological studies.

Sphincter disturbances were present in all patients in our cohort. Previous studies reported a proportion ranging from 53 to 94% (Kara et al., 2016; De Bot et al., 2013). De Bot et al. (2013) also reported fecal

incontinence, an uncommon feature in HSPs that was also present in our cohort. Approximately half of our patients manifested ataxia, while in precedent reports it ranged from 56 to 70% (Kara et al., 2016; Hehr et al., 2007; De Bot et al., 2013). It is relevant to stress that ataxia was a mild feature identified through subtle dysmetria and ataxic dysarthria. In opposition to what is found in the so called spastic-ataxias, where both symptoms are typically equally relevant, in SPG11 spasticity and weakness are the key aspects that lead to functional impairment (De Bot et al., 2013). Parkinsonism was seen in almost one third of our patients, but subtle hypomimia was a universal finding in this cohort. Nigrostriatal damage, revealed in the current study, probably underlies these manifestations. De Bot et al. (2013) stressed a high proportion of obesity among SPG11 patients, and hypothesized overweight was not secondary to immobility, but rather a phenotypic trait itself. Favoring that, the proportion of wheelchair bound patients in his cohort was actually higher among the non-obese. Neurodegenerative disorders like Huntington's disease and Spinocerebellar ataxias (Liot et al., 2017; Saute et al., 2012) are associated with unwanted weight loss, but in some disorders of the motor system, such as spinal muscular atrophy, the opposite takes place. Animal studies indicate SMN1 (survivor motor neuron 1) protein is implicated in glucose metabolism, increasing the risk of diabetes and obesity when *SMN1* gene is defective (Bowerman et al., 2014). Hence, it is possible that dysfunctional spastacsin may contribute to weight gain, but such hypothesis requires, however, further investigation.

Learning difficulties prior to the development of gait disturbance, were much more frequent in our study than previously reported by De Bot et al. (2013) (72% *vs* 39%). In the present cohort, extensive questioning in regard to behavioral and cognitive abnormalities was performed, what might have contributed to a higher diagnostic yield for learning disability. De Bot et al. (2013) suggested psychosis to be a phenotypic characteristic of SPG11; our findings are in line with this hypothesis since 16% of affected probands had history of hallucinations and/or delusional thoughts according to the caregivers output at the NPI. High rates of depression and anxiety were other neuropsychiatric hallmarks. An important aspect of SPG11 phenotypic characterization was the novel description of pathological laughter, a highly prevalent and characteristic trait that might be a diagnostic cue.

Dementia was diagnosed in 84% of our cohort and the cognitive deficits focused in executive, language and memory domains. The VLOM ratio as well as the high frequency of certain behavioral disturbances (abnormal agitation, disinhibition and apathy) strongly argued in favor of a preferential dysfunction of frontotemporal areas. In line with this finding is the description of hypometabolism in frontal lobes (Hehr et al., 2007) as well as pathological reports indicating preferential frontal lobe involvement (Denora et al., 2016). Inverse correlation of ACE-R with disease duration and age strongly supported the progressive nature of cognitive impairment, in opposition to a fixed mental handicap. Taken together, clinical and imaging data suggest that SPG11-related cognitive syndrome is indeed a developmental condition that is later followed by progressive decline. Dysfunction of frontotemporal regions plays a key role, but in contrast to the prototypical forms of frontotemporal lobar degenerations, cerebral cortex is disproportionately spared in comparison to basal ganglia and WM pathways. It thus seems that this is truly a subcortical type of frontotemporal dementia.

Concerning GM damage, volumetric reduction of the precentral gyri, basal ganglia and thalamus have been previously described (França Jr et al., 2012). Nonetheless, we were able to show that cortical thinning was more widespread than previously thought, affecting cingulum, STS, parahippocampal, paracentral and parietal regions. In regard to deep GM, we unraveled compromise of other relevant structures such as amygdala, substantia nigra, accumbens and red nucleus. Associative cortex thinning (SLS and left parietal regions) and thalamic volumetric reduction correlated directly with cognitive impairment. STS and parietal cortices play key roles in social cognition and spatial processing tasks, whereas thalamic regions are mainly implicated in memory and language skills (Deen et al., 2015; Klostermann et al., 2013; Jankowski et al., 2013). Functional MRI studies provide evidence that bilateral STS play a key role in social cognition, encompassing perception of biological motion, recognition of facial expressions, meaning of voice tone and understanding of other's actions and mental states (Deen et al., 2015). The parietal regions are activated during spatial processing tasks, such as for reaching or looking at a specific target. Whereas certain thalamic regions, such as the pulvinar and mediodorsal areas, are important modulators of neural processing. Their lesions are reported to produce a variety of cognitive deficits, mainly affecting language and memory skills (Klostermann et al., 2013; Jankowski et al., 2013). In addition to cognition, GM damage is also associated with motor manifestations. Paracentral and precentral thickness as well as putamens and accumbens nucleus volumes indeed correlated with motor severity. In terms of basal ganglia circuitry, our results point to diffuse compromise, involving not only the direct, but also the indirect pathway of movement control. These are probably the structural counterparts of parkinsonism, which is a frequent finding in SPG11 and reported in up to 30% of the cases (Anheim et al., 2009). Since regional atrophy was not restricted to the substantia nigra, but also involved the striatum, this suggests that treatment perspectives with levodopa or its agonists are scarce.

Concerning WM, we observed a widespread pattern of damage, in line with previous reports (França Jr et al., 2012; Pan et al., 2013). We were able to unfold neuropsychological correlates of WM integrity loss at the fornices and lateral portions of the corpus callosum (tapetum). The fornices connect the hippocampus to limbic structures and are important for episodic memory recall. Diffusivity abnormalities of the fornices are known to correlate with cognitive performance in various brain disorders such as Alzheimer's and Parkinson's diseases (Zheng et al., 2014; Mayo et al., 2016). Surprisingly, we failed to identify correlations between CST diffusivity measures and motor impairment. In contrast, SC morphometry indicated more significant atrophy in patients with longer disease duration. We hypothesize damage to other descending tracts in the SC might be implicated in the pathogenesis of the disease. Herein, volumetric analysis of the SC would provide a better representation, not of the CST alone, but of other motor pathways such as rubrospinal and reticulospinal tracts. One shall also consider that HSPs pathogenic mechanisms are related to disruption of intracellular axonal trafficking, resulting in particular vulnerability of distal tracts. When accessing MRI abnormalities, the SC is the most distal structure, responding to our correlation findings in regard to SC area and disease duration.

Peripheral nervous system (PNS) involvement has been noticed in SPG11 patients since the discovery of spastacsin mutations but it has not been systematically investigated in a larger group of patients before (Stevanin et al., 2007; Montecchiani et al., 2016; Manole et al., 2016). Manole et al. have performed the most comprehensive EMG study in SPG11 up to now. Despite the diagnosis of PNP in his cohort, taking a closer look at his data one can identify motor amplitudes were severely reduced, while there was no clear distal-proximal gradient, with CMAP obtained in the upper limbs being more significantly reduced than the ones obtained in lower limbs in three of the five affected individuals. SNAPS were absent in two patients with severe debilitating illness that also had significant feet edema. In the remaining patients sural responses were actually within normal range (range 6.9–11.6 μV). Jointly, the absence of distal-proximal gradient and the disproportionate sparing of SNAPS in relation to CMAPS argue strongly against PNP. In paraplegic patients, leg edema is a frequent complication that imposes a technical difficulty in obtaining SNAPS. It is probable that such challenge results in over diagnosing PNP in this group of patients. In the present cohort, NCS and needle EMG have strongly supported a primary affection of the cell bodies of the inferior motor neurons. Hence, whereas in the upper motor neuron a dying-back axonopathy is the primary mechanism leading to spastic paraparesis, concerning the

lower motor neuron the cell body is the primary site of damage in patients harboring *SPG11* mutations. This finding is in line with neuropathology of SPG11, which unfolds neuronal rarefaction and eosinophilic aggregates affecting the SC anterior horns (Denora et al., 2016). *SPG11* mutations are also an important cause of juvenile ALS, indicating spastacsin haploinsufficiency can result in various degrees of motor neuron disorder (Orlacchio et al., 2010). Additionally, we observed motor neuronopathy is a very frequent finding, affecting 96% of our cohort. De Bot et al. (2013) revealed *SPG11* mutations are associated with a more rapid clinical deterioration when compared to other HSP subtypes. Most patients become wheelchair bound after one or two decades of disease, while the few cases described in the fifth decade of life are tetraplegic and unable to speak. We hypothesize such an aggressive clinical course is related to the similarities SPG11 displays with ALS, on clinical, neurophysiological and neuropathological grounds.

Even though this was a transversal study, we have provided meaningful insights into the disease course. In regard to clinical aspects, we could demonstrate a progressive cognitive and motor dysfunction since these variables had a significant correlation with time-dependent variables. Moreover, we were able to determine the annual rate of progression based on a longitudinal clinical evaluation. On neuroimaging analyses, progressive dysfunction of GM and SC contrasted with an apparently static WM involvement. The lack of correlation between time-related measures and DTI metrics could be attributed to a neurodevelopmental disorder of the WM. Alternatively, a very early degeneration of WM could lead to a ceiling effect when evaluating adults, what could be better elucidated by future prospective studies, ideally with younger probands.

Through neurophysiologic studies, we could reveal that a motor neuronopathy, similar to what is identified in spinal muscular atrophy or in slowly progressive cases of ALS, is a major feature of SPG11.

Altogether, these findings in association with the presence of frequent cognitive (72%) and motor difficulties (25%) prior to the establishment of the full clinical picture argue in favor of two concurrent processes: a neurodevelopmental disorder associated with subsequent neurodegenerative process. In fact, studies with the zebrafish knockout model of SPG11 support the role of spastacsin during neuronal development (Southgate et al., 2010). Neuropathological investigation, on the other hand, unfolds signs of degeneration such as neuronal loss and gliosis (Denora et al., 2016).

In conclusion, we were able to unravel the phenotypic and structural hallmarks of SPG11. In brief, it seems that GM and WM matter are distinctly affected in the disease, not only in terms of extension but also in terms of temporal course. Our data strongly support the concept that spatacsin-related neurodegeneration is characterized by selective neuronal vulnerability. Basal ganglia are disproportionately involved and take part in key clinical features of the disease, such as movement disorders and dementia. Motor neuronopathy also seems to be a major feature, reinforcing the link between HSP and ALS in relation to neurodegeneration topography. Future larger and prospective studies are warranted to better elucidate the natural history of disease.

Acknowledgements

We would like to acknowledge the support provided by the São Paulo Research Foundation, FAPESP (Grant 2013/017667 to MCFJr), the Brazilian National Council for Scientific and Technological Development (grant #303914/2014-9), CNPq and the Italian Ministero della Salute (Grant no. GR09.109 to AO).

Appendix A. Supplementary data

Supplementary data to this article can be found online at https://doi.org/10.1016/j.nicl.2018.05.031.

References

Agosta, F., Ferraro, P.M., Riva, N., Spinelli, E.G., Chiò, A., Canu, E., et al., 2016. Structural brain correlates of cognitive and behavioral impairment in MND. Hum. Brain Mapp. 37, 1614–1626.
Anheim, M., Lagier-Tourenne, C., Stevanin, G., et al., 2009. SPG11 spastic paraplegia. A new cause of juvenile parkinsonism. J. Neurol. 256, 104–108.
Bowerman, M., Michalski, J.P., Beauvais, A., Murray, L.M., De Repentigny, Y., Kothary, R., 2014. Defects in pancreatic development and glucose metabolism in SMN – depleted mice independent of canonical spinal muscular atrophy neuromuscular pathology. Hum. Mol. Genet. 23, 3432–3444.
Branco, L.M., De Albuquerque, M., De Andrade, H.M., Bergo, F.P., Nucci, A., França Jr., M.C., 2014. Spinal cord atrophy correlates with disease duration and severity in amyotrophic lateral sclerosis. Amyotroph Lateral Scler. Frontotemporal Degener. 15, 93–97.
Carvalho, V.A., Caramelli, P., 2007. Brazilian adaptation of the Addenbrooke's Cognitive Examination-Revised (ACE-R). Dement. Neuropsychol. (2), 212–216.
Cummings, J.L., Mega, M., Gray, K., Rosenberg-Thompson, S., Carusi, D.A., Gornbein, J., 1994. The neuropsychiatric inventory: comprehensive assessment of psychopathology in dementia. Neurology 44, 2308–2314.
De Bot, S.T., Burggraaff, R.C., Herkert, J.C., et al., 2013. Rapidly deteriorating course in Dutch hereditary spastic paraplegia type 11 patients. Eur. J. Hum. Genet. 21, 1312–1315.
De Rezende, T.J.R., D'Abreu, A., Guimarães, R.P., Lopes, T.M., Lopes-Cendes, I., Cendes, F., et al., 2015. Cerebral cortex involvement in Machado Joseph disease. Eur. J. Neurol. 22, 277–283.
Deen, B., Koldewyn, K., Kanwisher, N., Saxe, R., 2015. Functional organization of social perception and cognition in the superior temporal sulcus. Cereb. Cortex 25, 4596–4609.
Denora, P.S., Smets, K., Zolfanelli, F., et al., 2016. Motor neuron degeneration in spastic paraplegia 11 mimics amyotrophic lateral sclerosis lesions. Brain 139, 1723–1734.
Desikan, R.S., Segonne, F., Fischl, B., Quinn, B.T., Dickerson, B.C., Blacker, D., et al., 2006. An automated labeling system for subdividing the human cerebral cortex on MRI scans into gyral based regions of interest. NeuroImage 31, 968–980.
Faber, I., Prota, J.R., Martinez, A.R., Lopes-Cendes, I., França Jr., M.C., 2017. A new phenotype associated with homozygous GRN mutations: complicated spastic paraplegia. Eur. J. Neurol. 24, e3–e4.
Fischl, B., Dale, A.M., 2000. Measuring the thickness of the human cerebral cortex from magnetic resonance images. Proc. Natl. Acad. Sci. U. S. A. 97, 11050–11055.
França Jr., M.C., D'Abreu, A., Nucci, A., Lopes-Cendes, I., 2008. Muscle excitability abnormalities in Machado-Joseph disease. Arch. Neurol. 65, 525–529.
França Jr., M.C., Yasuda, C.L., Pereira, F.R., D'Abreu, A., Lopes-Ramos, C.M., Rosa, M.V., et al., 2012. White and grey matter abnormalities in patients with SPG11 mutations. J. Neurol. Neurosurg. Psychiatry 83, 828–833.
Hamosh, A., Sobreira, N., Hoover-Fong, J., et al., 2013. PhenoDB: a new web-based tool for the collection, storage, and analysis of phenotypic features. Hum. Mutat. 34, 566–571.
Hanganu, A., Bedetti, C., Degroot, C., Mejia-Constain, B., Lafontaine, A.L., Soland, V., et al., 2014. Mild cognitive impairment is linked with faster rate of cortical thinning in patients with Parkinson's disease longitudinally. Brain 137, 1120–1129.
Harding, A.E., 1983. Classification of the hereditary ataxias and paraplegias. Lancet 1, 1151–1155.
Hehr, U., Bauer, P., Winner, B., et al., 2007. Long-term course and mutational spectrum of spatacsin-linked spastic paraplegia. Ann. Neurol. 62, 656–665.
Hutton, C., Draganski, B., Ashburner, J., Weiskopf, N., 2009. A comparison between voxel-based cortical thickness and voxel-based morphometry in normal aging. NeuroImage 48, 371–380.
Jankowski, M.M., Ronnqvist, K.C., Tsanov, M., et al., 2013. The anterior thalamus provides a subcortical circuit supporting memory and spatial navigation. Front. Syst. Neurosci. 7, 45.
Jiang, H., van Zijl, P.C., Kim, J., et al., 2006. DTIStudio: resource program for diffusion tensor computation and fiber bundle tracking. Comput. Methods Prog. Biomed. 81, 106–116.
Kara, E., Tucci, A., Manzoni, C., et al., 2016. Genetic and phenotypic characterization of complex hereditary spastic paraplegia. Brain 139, 1904–1918.
Klostermann, F., Krugel, L.K., Ehlen, F., 2013. Functional roles of the thalamus for language capacities. Front. Syst. Neurosci. 7, 32.
Liot, G., Valette, J., Pépin, J., Flament, J., Brouillet, E., 2017. Energy defects in Huntington's disease: why “in vivo” evidence matters. Biochem. Biophys. Res. Commun. 483, 1084–1095.
Manole, A., Chelban, V., Haridy, N.A., et al., 2016. Severe axonal neuropathy is a late manifestation of SPG11. J. Neurol. 263, 2278–2286.
Mayo, C.D., Mazerolle, E.L., Ritchie, L., Fisk, J.D., Gawryluk, J.R., 2016. Longitudinal changes in microstructural white matter metrics in Alzheimer's disease. Neuroimage Clin. 13, 330–338.
Menon, P., Kiernan, M.C., Yiannikas, C., Stroud, J., Vucic, S., 2013. Split-hand index for the diagnosis of amyotrophic lateral sclerosis. Clin. Neurophysiol. 124, 410–416.
Miller, M.I., Faria, A.V., Oishi, K., Mori, S., 2013. High-throughput neuroimaging informatics. Front Neuroinform. 17, 7–31.
Mioshi, E., Dawson, K., Mitchell, J., Arnold, R., Hodges, J.R., 2006. The Addenbrooke's Cognitive Examination Revised (ACE-R): a brief cognitive test battery for dementia screening. Int. J. Geriatr. Psychiatry 21, 1078–1085.
Montecchiani, C., Pedace, L., Lo Giudice, T., et al., 2016. SPG11 mutations cause autosomal recessive axonal Charcot-Marie-tooth disease. Brain 139, 73–85.
Oberbeek, B., van Alfen, N., Bor, J.A., Zwarts, M.J., 2005. Sural/radial nerve amplitude

ratio: reference values in healthy subjects. Muscle Nerve 32, 613–618.
Orlacchio, A., Babalini, C., Borreca, A., Patrono, C., Massa, R., Basaran, S., et al., 2010. SPATACSIN mutations cause autosomal recessive juvenile amyotrophic lateral sclerosis. Brain 133, 591–598.
Pan, M.K., Huang, S.C., Lo, Y.C., D'Abreu, A., Lopes-Ramos, C.M., Rosa, M.V., et al., 2013. Microstructural integrity of cerebral fiber tracts in hereditary spastic paraparesis with SPG11 mutation. AJNR Am. J. Neuroradiol. 34, 990–996.
Pensato, V., Castellotti, B., Gellera, C., Pareyson, D., Ciano, C., Nanetti, L., et al., 2014. Overlapping phenotypes in complex spastic paraplegias SPG11, SPG15, SPG35 and SPG48. Brain 137, 1907–1920.
Richards, S., Aziz, N., Bale, S., et al., 2015. Standards and guidelines for the interpretation of sequence variants: a joint consensus recommendation of the American College of Medical Genetics and Genomics and the Association for Molecular Pathology. Genet. Med. 17, 405–424.
Rutkove, S.B., Kothari, M.J., Raynor, E.M., Levy, M.L., Fadic, R., Nardin, R.A., 1997. Sural/radial amplitude ratio in the diagnosis of mild axonal polyneuropathy. Muscle Nerve 20, 1236–1241.
Saute, J.A., Silva, A.C., Souza, G.N., Russo, A.D., Donis, K.C., Vedolin, L., et al., 2012. Body mass index is inversely correlated with the expanded CAG repeat length in SCA3/MJD patients. Cerebellum 11, 771–774.
Schüle, R., Holland-Letz, T., Klimpe, S., Kassubek, J., Klopstock, T., Mall, V., et al., 2006. The Spastic Paraplegia Rating Scale (SPRS): a reliable and valid measure of disease severity. Neurology 67, 430–434.
Siri, L., Battaglia, F.M., Tessa, A., Rossi, A., Rocco, M.D., Facchinetti, S., et al., 2010. Cognitive profile in spastic paraplegia with thin corpus callosum and mutations in SPG11. Neuropediatrics 41, 35–38.
Southgate, L., Dafou, D., Hoyle, J., Li, N., Kinning, E., Critchley, P., 2010. Novel SPG11 mutations in Asian kindreds and disruption of spatacsin function in the zebrafish. Neurogenetics 11, 379–389.
de Souza, P.V., de Rezende Pinto, W.B., de Rezende, G.N.B., Bortholin, T., Oliveira, A.S.B., 2017. Hereditary spastic paraplegia: clinical and genetic hallmarks. Cerebellum 16, 525–551.
Stevanin, G., Santorelli, F.M., Azzedine, H., Coutinho, P., Chomilier, J., Denora, P.S., et al., 2007. Mutations in SPG11, encoding spatacsin, are a major cause of spastic paraplegia with thin corpus callosum. Nat. Genet. 39, 366–372.
Tang, X., Shoko, Y., Hsu, J., et al., 2014. Multi-contrast multi-atlas parcellation of diffusion tensor imaging of the human brain. PLoS One 9, e96985.
Towns, J., Cockerill, T., Dahan, M., 2014. XSEDE: accelerating scientific discovery. Comput. Sci. Eng. 16, 62–72.
Wu, D., Ma, T., Ceritoglu, C., et al., 2016. Resource atlases for multi-atlas brain segmentations with multiple ontology levels based on T1-weighted MRI. NeuroImage 125, 120–130.
Zheng, Z., Shemmassian, S., Wijekoon, C., Kim, W., Bookheimer, S.Y., Pouratian, N., 2014. DTI correlates of distinct cognitive impairments in Parkinson's disease. Hum. Brain Mapp. 35, 1325–1333.
Zhuang, J., Hrabe, J., Kangarlu, A., et al., 2006. Correction of eddy–current distortions in diffusion tensor images using the known directions and strengths of diffusion gradients. J. Magn. Reson. Imaging 24, 1188–1193.